Phase and microstructural development of sol-gel-derived strontium barium niobate thin films

A.Y. Oral and M.L. Mecartney
Department of Chemical and Biochemical Engineering and Materials Science, University of California—Irvine, Irvine, California 92697-2575

(Received 18 October 1999; accepted 22 March 2000)

Microstructural changes in sol-gel-derived $Sr_xBa_{1-x}Nb_2O_6$ (SBN) thin films were monitored as a function of Ba-to-Sr ratio (from $x = 0$ to $x = 1$), choice of substrate (Si or MgO), and processing variations. Sols were created using Ba, Sr, and Nb alkoxides dissolved in acetic acid. The relatively high decomposition temperature for the organics led to a tendency to form defects, but careful control of thermal process parameters could be used to produce a uniform film microstructure. An unexpected phase, interpreted as a hexagonal (pseudo-orthorhombic) variant of hexagonal $BaNb_2O_6$, was encountered in Ba-rich sol-gel-derived SBN powders and thin films annealed at 750 °C. Increased (001) orientation was observed for SBN thin films deposited on (100) MgO when fast thermal processing was used.

I. INTRODUCTION

Strontium barium niobate ($Sr_xBa_{1-x}Nb_2O_6$, SBN) is a ferroelectric phase with a tungsten bronze structure that is formed between $BaNb_2O_6$ and $SrNb_2O_6$. The region of solid solution for the tungsten bronze structure is generally accepted to be $0.25 < x < 0.75$.[1] Two different lattice types and symmetries have been observed in the solid solution. The first phase is tetragonal, with space group *P4bm*, having approximate lattice parameters of $a,b = 1.24$ nm, $c = 0.39$ nm. Numerous members of the ferroelectric tungsten bronze type of oxides all have a related tetragonal symmetry with a unit cell of approximately 1.2 × 12 × 0.39 nm containing 10 corner-sharing MO_6 (M = penta valent cation) octahedra.[2] The tungsten bronze structure is a layered type, with the oxygen ions forming slightly puckered sheets at approximately $z = 0$ and ½, the M ions at approximately $z = 0$ and the remaining cations (Ba, Sr, Na, etc.) at $z = ½$.

A closely related structure to the tetragonal tungsten bronze family has orthorhombic symmetry, with a unit cell of approximately 1.75 × 1.75 × 0.8 nm. The orthorhombic variant is related to the tetragonal unit cell by the following equations:

$$a_{\text{orth}} \cong b_{\text{orth}} \cong \sqrt{2}a_{\text{tetragonal}} \quad , \tag{1}$$

$$c_{\text{orth}} \cong 2c_{\text{tetr}} \quad . \tag{2}$$

Only a few researchers have identified this orthorhombic structure (space group *Cmm*2) in the $BaNb_2O_6$–$SrNb_2O_6$ system and assigned approximate lattice parameters, $a,b = 1.76$ nm, $c = 0.78$.[3–6]

The basic formula for a ferroelectric tetragonal tungsten bronze is $[(A1)_2\ (A2)_4\ C_4]\ [(M1)_2\ (M2)_8]\ O_{30}$.[2] The skeletal framework of the tungsten bronze structure is formed by MO_6 octahedra, which share corners to form cavities of A1, A2, and C (Fig. 1). The smaller cations prefer A1 sites because of the relatively smaller size of A1 sites compared to A2 sites. Jamieson and Bernstein's[5] atom distribution model for SBN suggests that Ba cations are only found in large A2 sites and Sr atoms preferably occupy the small A1 sites. Nevertheless, some of the Sr atoms can also occupy A2 sites, especially in Sr-rich solid solutions. The C site is the smallest of the three cavities created by the framework of octahedra. Very small cations that may occupy the C site are lithium, vanadium, and beryllium.[1]

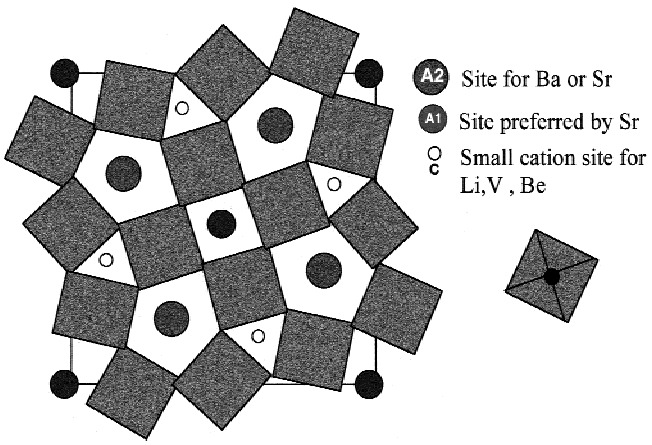

FIG. 1. The tetragonal tungsten bronze structure. Niobium sits in the center of the oxygen octahedra.

$Sr_xBa_{1-x}Nb_2O_6$ is a ferroelectric material. Below the Curie temperature, all the cations are displaced offset from the planes of oxygen atoms along the *c* axis, resulting in maximum polarization along the [001] direction. At thermodynamic equilibrium, when $x = 0.67$, Sr ions are in the A1 sites and Ba ions are at A2 sites. As the Sr content (x) of the solution increases, SBN changes from a normal ferroelectric to a relaxor ferroelectric. During this transition, as the Ba content decreases, the Sr/Ba ratio in the A2 sites increases.[1] The Sr atoms in A2 sites may be responsible for the broadening of the temperature range for the paraelectric to ferroelectric transition, inducing relaxor behavior.

The metaniobates, $BaNb_2O_6$ and $SrNb_2O_6$, that are the end compositions of the SBN phase diagram are not ferroelectric although their chemical formulae are similar to SBN. The relative positions of the octahedra in the crystal structure determine whether a compound is ferroelectric or not. In these metaniobates, the octahedra meet along their edges.[3] In all known ferroelectrics, the octahedra only join at their vertices and it is believed that this type of array is responsible for the strong internal fields in the crystals. The size of the A^{+2} cation appears to be the main factor determining the relative positions of the octahedra. In metaniobate solid solutions, only if the mean radius of the A^{+2} cations is close to radius of Pb, should the solid solution possess ferroelectric properties ($PbNb_2O_6$ is the only known ferroelectric metaniobate).[7]

The experiments described in this paper examine the low-temperature crystallization of a range of $Sr_xBa_{1-x}Nb_2O_6$ compositions from $x = 0$ ($BaNb_2O_6$) to $x = 1$ ($SrNb_2O_6$) using a modified sol-gel approach.

II. EXPERIMENTAL PROCEDURE

Figure 2 illustrates the material preparation process. A new type of sol was prepared by dissolving Ba–isopropoxide and Sr–isopropoxide in acetic acid and mixing with Nb–ethoxide. In previous studies,[8,9] ethanol was commonly used as a solvent for the preparation of the sol-gel-derived SBN thin films. These sols are difficult to prepare due to their high sensitivity to the moisture in air.[4] This modified sol preparation method, using acetic acid as a main solvent, eliminates these problems, because acetic acid is a suitable chelating agent reducing the susceptibility of sols to fast hydrolysis. The new sols have a very low sensitivity to moisture and a shelf life of several months. Furthermore, preparation of the new sols requires only 20 min whereas ethanol-based sols can require many hours.

The final solution, with a concentration of 0.36 M, was light brown and clear without any suspension of particles. The solutions were spun at 2000 rpm for 60 s onto (111) Si and (100) MgO substrates. After five layers of coating, the films were approximately 500 nm thick.

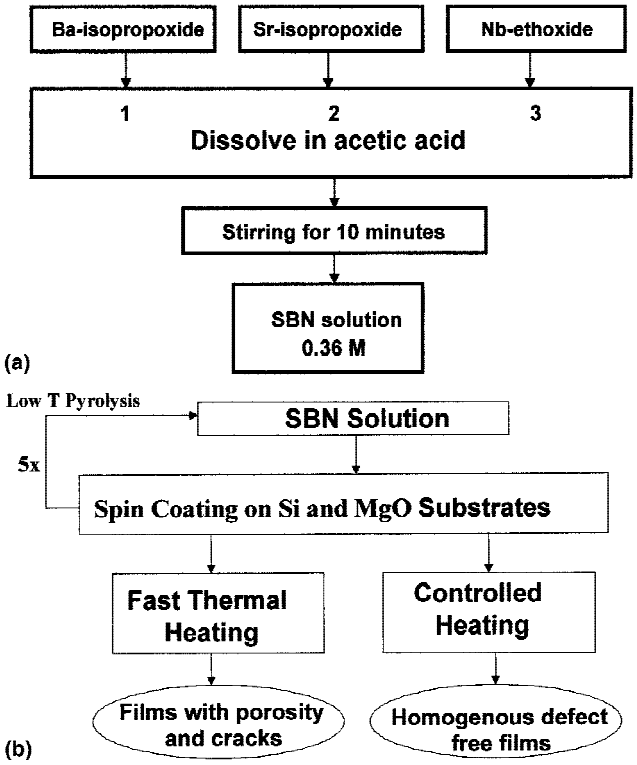

FIG. 2. Flow chart of (a) sol preparation and (b) film fabrication.

Two different heat-treatment methods were used to crystallize the thin films. The first one was fast thermal processing. In this process, a pyrolysis heat treatment was applied to each layer of the films at 350 °C following deposition. After the last coating was applied, the films were directly inserted into the furnace at 750 °C and heat treated for 60 min. Powders were also produced by drying the sols in open containers in the atmosphere followed by fast thermal processing and a heat treatment at 750 °C for 60 min.

The second heat treatment method was controlled furnace annealing, which used the information obtained from thermogravimetric analysis (TGA) to determine various heating rates applied during annealing. Heating rates as slow as 1 °C/min were used in regions corresponding to sharp weight losses identified in the TGA curves. In addition, the temperature was held for 60 min at the midpoints of every temperature range with a major weight loss (Fig. 3). The crystal structures and the crystallization behaviors of the films and powders were analyzed by x-ray diffraction (XRD) using a Siemens D5000 apparatus, transmission electron microscopy (TEM) using a Philips CM20 apparatus, differential scanning calorimetry (DSC), and TGA. Surface morphology of the films was examined by scanning electron microscopy (SEM) with a Philips XL 30 FEG apparatus.

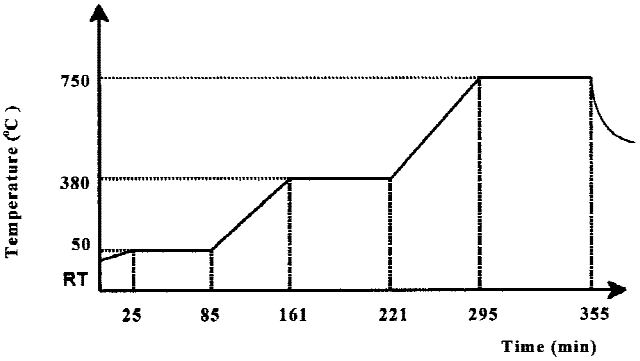

FIG. 3. Heating profile for the controlled furnace annealing.

III. RESULTS AND DISCUSSION

A. Effect of heat treatment on microstructural development

DSC and TGA results indicate that crystallization occurs around 535 °C, represented by a strong exothermic peak at 535 °C in the DSC graphs with no corresponding weight loss in the TGA analysis. In addition are three temperature ranges associated with weight losses. The first weight loss, extending from room temperature to around 150 °C, also represented by an endothermic peak in DSC, should be caused by evaporation of solvents. A second sharp weight loss between 300 and 400 °C, matched by an exothermic peak in DSC graphs, is possibly caused by the burnout of organics. A final weight loss at temperatures between 710 and 730 °C is most likely caused by the decomposition of bound organics and the combustion of free carbon in the films and is accompanied by exothermic peaks in the DSC. The weight loss between 710 and 730 °C is significantly less when slower heating rates are used (5% weight loss with a heating rate of 10 °C/min and 0.5% weight loss with a heating rate of 5 °C/min).

SBN50 films on Si substrates exhibited substantial microstructural variations when different heating rates were applied during annealing. The films produced by fast thermal processing were full of cracks and bubbles (Fig. 4). In contrast, films that were produced by controlled furnace annealing, at slow heating rates, were uniform and defect free on a macroscopic scale (Fig. 5). The bubbles in the fast thermal processing films are likely caused by entrapped gases between the substrate and the film during the decomposition of organics and the combustion of free carbon at higher temperatures. The macroscopic voids seen in the SEM micrographs may be developed by fast solvent evaporation at low temperatures. Cracks form due to the rapid shrinkage of the film during rapid heating. Abrupt temperature changes during fast thermal processing enhance the crack formation. Films produced by controlled furnace annealing did not contain macroscopic voids due to slower decomposition and evaporation at lower temperatures.

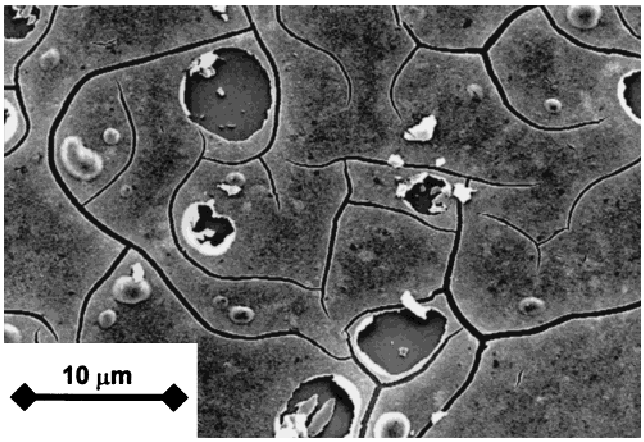

(a)

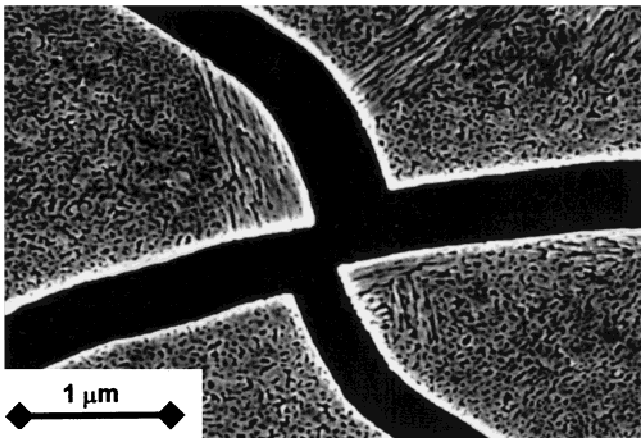

(b)

FIG. 4. Scanning electron micrographs of SBN50 film deposited on (111) Si substrates prepared by fast thermal processing: (a) the presence of voids and cracks seen at lower magnifications, (b) nanoscale porosity evident at higher magnifications.

All films, however, contained nanometer-scale porosity. TEM micrographs show that the regions in Fig. 5(b), defined by a uniform orientation of the elongated nanoporosity, correspond to single grains (Fig. 6). The orientation of the pores appears to be related to the crystal anisotropy because the pores are elongated in the same direction inside each grain.

B. Crystalline phases

Four different crystalline phases were formed throughout the solid solution ($0 \leqslant x \leqslant 1$). The same phases were found after annealing at 750 °C for both thin films and powders (Figs. 7 and 8). Orthorhombic $BaNb_2O_6$ was identified near the Ba-rich end, as predicted by the equilibrium phase diagram [Fig. 7(a)]. An unexpected crystal structure was identified in films and powders that had a small amount of Sr [Figs. 7(b) and 8(a)]. This new phase, which has been previously identified as an orthorhombic tungsten bronze phase by some researchers,[4,9] exists as a single phase at intermediate Sr values ($0.15 \leqslant x \leqslant 0.45$).

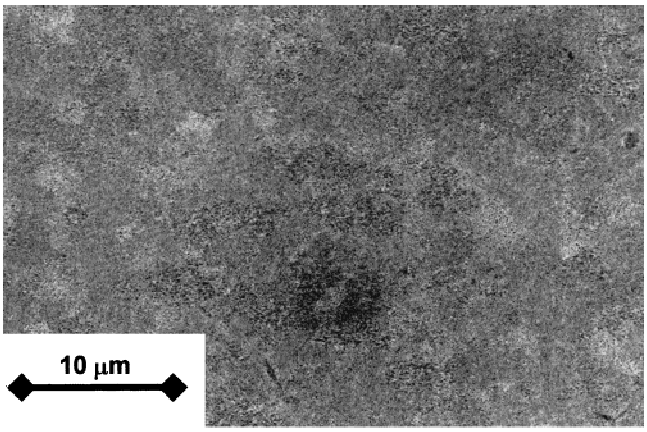

FIG. 5. Scanning electron micrographs of SBN50 film deposited on (111) Si substrate prepared by controlled furnace annealing: (a) uniform microstructure observed at low magnifications, (b) nanoscale porosity with grainlike regions evident at higher magnifications.

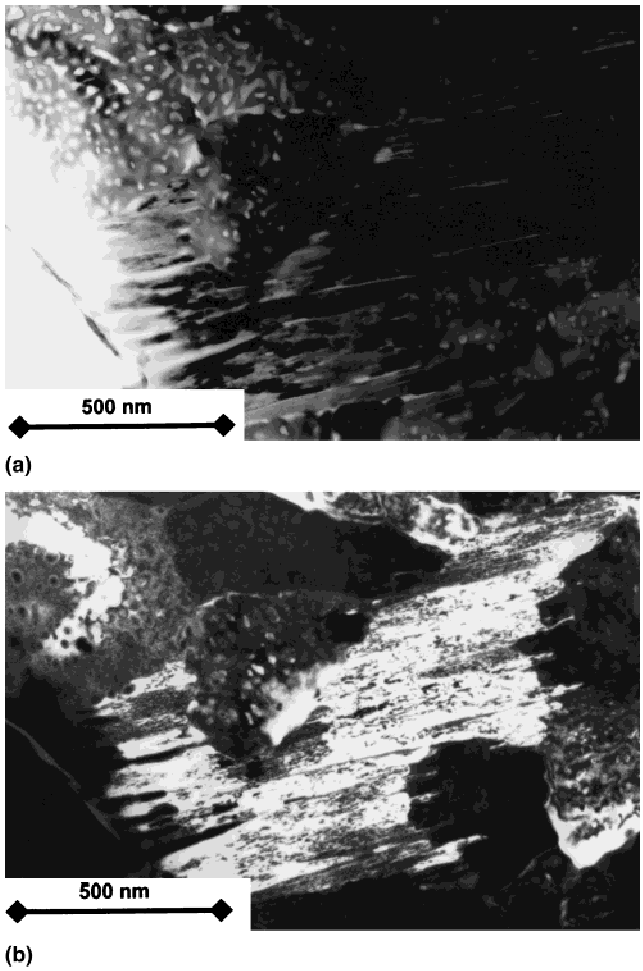

FIG. 6. (a) Bright-field TEM image of SBN50 thin films on (111) Si substrate. (b) Dark-field TEM image of SBN50 thin films on (111) Si substrate. Regions with similarly oriented porosity are single grains.

This unexpected phase has *d* spacings and intensities similar to hexagonal (pseudo-orthorhombic) $BaNb_2O_6$. Barium metaniobate, $BaNb_2O_6$, has two polymorphs: orthorhombic and hexagonal. The hexagonal structure is a sheared version of the tetragonal tungsten bronze structure with some edge-sharing octahedra replacing corner sharing. The hexagonal form is a metastable structure between the orthorhombic structure and tungsten bronze structure and has been found when alkoxides are used to produce barium metaniobate at low temperatures.[10] Sol-gel systems involve nonequilibrium processing, and when metal alkoxides are used, there can be a correlation between the structure of the molecular units in the sol and gel form and the final crystal structure.[8] Major structural changes can be inhibited due to insufficient thermal energy at the very low calcination temperatures used in sol-gel processing. Strong chemical bonds form in the metal oxides after the removal of organics and nonequilibrium phases can result. The hexagonal form of barium metaniobate, produced from alkoxides, transforms to the orthorhombic modification when heated up to 1250–1310 °C.[10] During cooling, the orthorhombic-to-hexagonal transformation does not occur, which indicates that the transformation is irreversible and the hexagonal phase is metastable.[10] The unexpected SBN phase identified here for $0.15 \leqslant x \leqslant 0.45$ may be a distorted version of the hexagonal $BaNb_2O_6$ structure with Ba ions replaced by smaller Sr ions.

Around the middle of solid solution ($x = 0.5$), the tetragonal tungsten bronze phase starts to form [Figs. 7(c) and 8(b)]. The reason for this transformation should be the increasing instability of the hexagonal (pseudo-orthorhombic) $BaNb_2O_6$ structure due to increasing concentration of smaller Sr ions. The $BaNb_2O_6$ structure has only one single-size interstitial site (large). When two different cations (Ba,Sr) with a considerable size difference are present in the equilibrium concentration, the tungsten bronze structure with different sizes of interstitial sites becomes the most stable structure due to the reduction of strain in the structure. In these sol-gel-

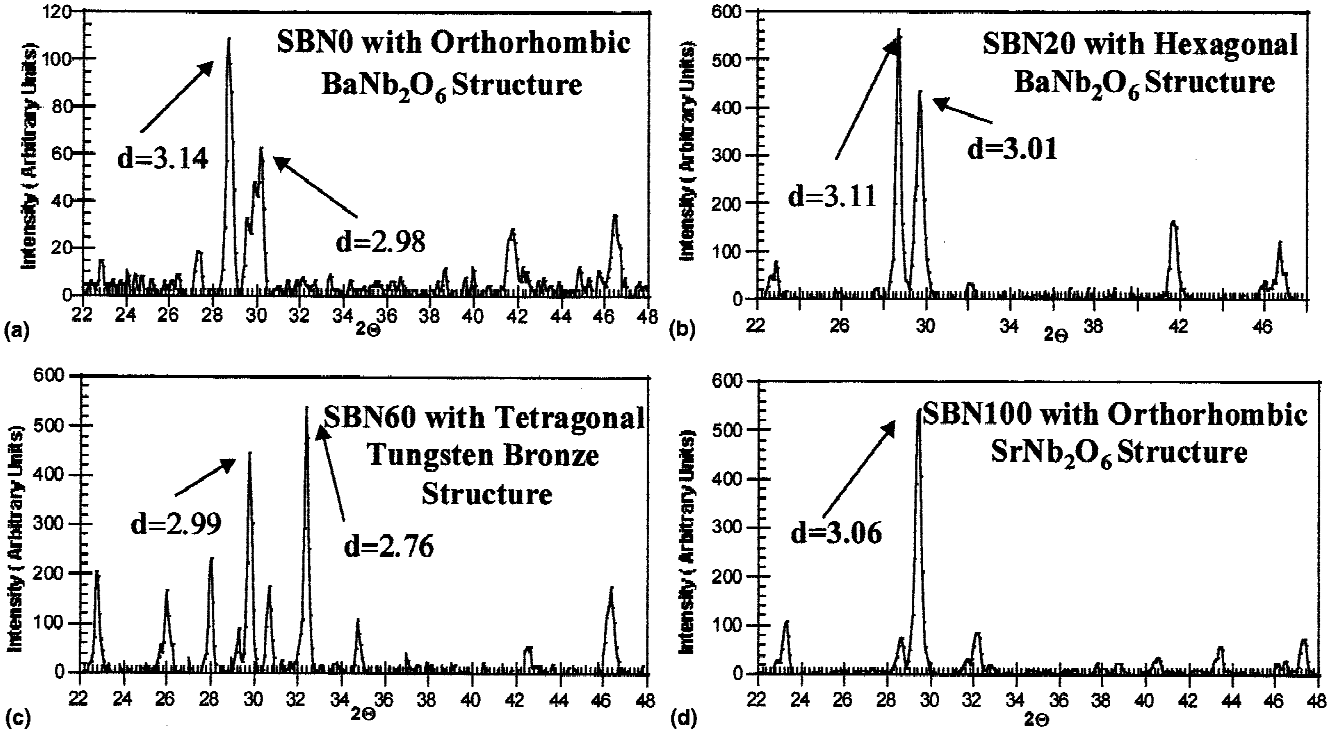

FIG. 7. XRD patterns of SBN powders: (a) BN, (b) SBN20, (c) SBN60, and (d) SN.

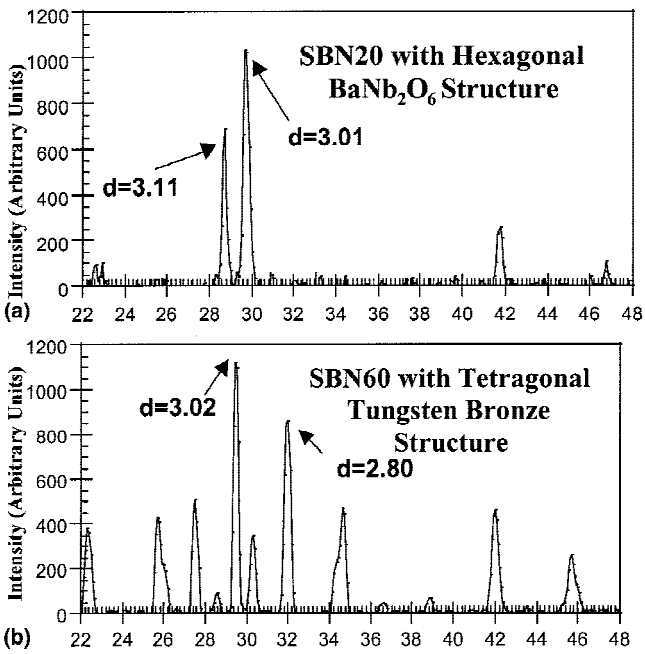

FIG. 8. XRD patterns of SBN thin films (a) SBN20 and (b) SBN60.

derived materials, the tetragonal tungsten bronze phase was found to exist as a single phase only in a narrow composition range around $x = 0.65$.

Near the $SrNb_2O_6$ end ($0.85 \leqslant x$), the equilibrium orthorhombic $SrNb_2O_6$ phase (isostructural with $CaTa_2O_6$) was identified [Figure 7(d)]. As the number of large Ba ions decreases, the need for the large interstitial sites also decreases and the orthorhombic $SrNb_2O_6$ structure with smaller interstitial sites becomes more stable than the tetragonal tungsten bronze structure. The phase diagram for SBN powders and thin films after low-temperature processing at 750 °C is summarized in Fig. 9.

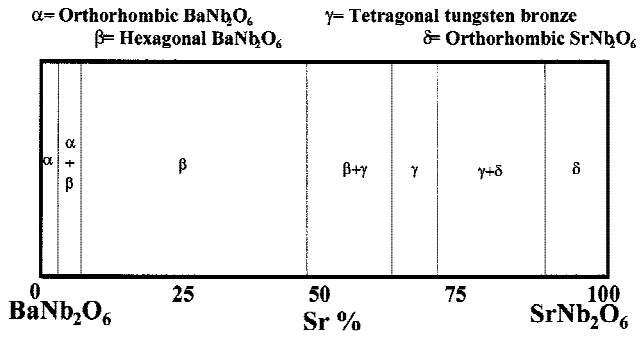

FIG. 9. An approximate phase diagram for SBN solid solutions after annealing sol-gel-derived SBN at 750 °C.

The new low-Sr phase of SBN found in this work and identified as a hexagonal (pseudo-orthorhombic) phase based on the diffraction match with hexagonal BN has been previously attributed to the incommensurate high-temperature orthorhombic phase of SBN that occurs in single crystals grown from the melt.[6] It is unlikely, however, that the incommensurate orthorhombic structure encountered in single crystals is the same as the phase identified in this paper as the low-temperature hexagonal

(pseudo-orthorhombic) phase of SBN formed after sol-gel processing. Single crystals are produced at high temperatures ($T > 1400$ °C) from liquid SBN and should represent an equilibrium high-temperature phase. The low-temperature phase identified here is metastable and transforms to the tetragonal tungsten bronze structure after annealing at 1200 °C.

Francombe[11] has reported that there is a slope change in the lattice parameter shift at $x = 0.45$ for single-crystal SBN as the Sr/Ba ratio of the solid solution is varied. This slope change may be due to the formation of a new phase. Carruthers and Grasso[12] detected an orthorhombic splitting of the diffraction peaks in SBN barium-rich solid solutions of SBN ceramics ($x < 0.45$). In this current work, a nontetragonal tungsten bronze phase also exists as a single phase in solid solutions with $x < 0.45$, but the *d* spacings of this phase do not match the orthorhombic splitting observed by Carruthers and Grasso.[12] TEM high-resolution lattice images obtained from the low-temperature hexagonal (pseudo-orthorhombic) phase (Fig. 10) include a lattice spacing of 0.84 nm that does not match the orthorhombic phase.

An orthorhombic distortion in barium-rich solid solutions ($x < 0.5$) of SBN single crystals has also been observed by Bursill and Lin[13,14] and Viehland *et al.*[6] This orthorhombic structure has a uniform mixing of blocks of two orthorhombic cells with lattice parameters $a = 17.58$Å, $b = 35.16$Å, $c = 7.83$Å and $a = 17.58$Å, $b = 17.58$Å, $c = 7.83$Å in the ratio of 3:1.[6,13,14] The incommensurate structure forms due to shearing of oxygen octahedra in the *a–b* plane. In the results presented here, there is no evidence of the large *d* spacings that should be present in diffraction patterns of the high-temperature orthorhombic phase.[13,14]

However, Sakamato *et al.*[9] have suggested that the unknown phase in sol-gel-derived SBN50 powders annealed at 700 °C should be orthorhombic. Their unknown phase transformed to a tetragonal tungsten bronze structure when annealed at 1200 °C, similar to the transformation found in our experiments. The main diffraction peak in the XRD patterns, around $2\Theta = 30°$, shifted from the main lattice spacing of BN to SN as the Sr content increased. From this shift the researchers suggested that a possible orthorhombic solid solution could form between BN and SN at low temperatures.[9] Although similar peak shifts were also encountered in the work reported here, a distinct tetragonal tungsten bronze phase was found to form in Sr-rich solid solutions. In addition, it should be noted that the crystal structures of $BaNb_2O_6$ and $SrNb_2O_6$ are not isostructural, so complete solid solubility is not possible.

The hexagonal (pseudo-orthorhombic) structure encountered in SBN thin films and powders, produced by sol-gel processing, could be a distorted version of hexagonal $BaNb_2O_6$ due to the replacement of Ba ions by Sr ions. The thermal energy supplied by the annealing at 750 °C may be insufficient to rearrange the local orientation of edge-sharing Nb–O octahedra to form corner-sharing Nb–O octahedra as required by the tetragonal tungsten bronze structure. Annealing at higher temperatures (1200 °C) supplies more thermal energy and results in the formation of the equilibrium tetragonal tungsten bronze structure. It should also be noted that due to the edge sharing of Nb–O octahedra in the hexagonal (pseudo-orthorhombic) structure, it is unlikely that this metastable SBN phase is ferroelectric.

C. Orientation

Thin films grown on (111) Si had a random orientation, with thin-film diffraction patterns similar to the powders (Figs. 7 and 8). Oriented ferroelectric thin films, however, are highly desired, because larger values of remnant polarizations can be obtained.[14]

The use of (100) MgO substrates enhanced for formation of the tetragonal tungsten bronze phase [Fig. 11(a)]. There is a close lattice matching of three unit cells of (100) MgO ($a = 0.42$ nm) with the (100) and the (010) planes of the SBN tetragonal tungsten bronze structure. The lattice mismatch ranges from 1.8% to 1.3% as the Sr content of the solution decreases from $x = 0.75$ to $x = 0.25$. In these experiments single-phase tetragonal tungsten bronze could be formed at $x = 0.73$ on (100) MgO while the orthorhombic SN phase began to form for SBN thin films on Si substrates.

Despite the close lattice match, no apparent grain orientation was observed on MgO when the films were produced by controlled furnace annealing. In contrast, a strong preferred (001) orientation was apparent for the films produced by fast thermal processing [Fig. 11(b)]. This different in grain orientation suggests that the role of the substrate is more pronounced at higher heating rates, possibly due to the initiation of crystallization at the substrate–film interface and some degree of epitaxial growth. However, the faster crystallization also introduced some of the orthorhombic $SrNb_2O_6$ phase.

IV. CONCLUSIONS

(1) Good quality SBN thin films can be produced by sols made by dissolution of alkoxides in acetic acid.

(2) The heating rate is a key aspect to the film quality. Controlled slow heating rates with holds at the decomposition temperatures allow decomposition reactions to occur at lower temperatures and sintering at higher temperatures to produce defect-free films.

(3) Two orthorhombic structures, a hexagonal (pseudo-orthorhombic) structure, and one tetragonal tungsten bronze crystal structure were identified through-

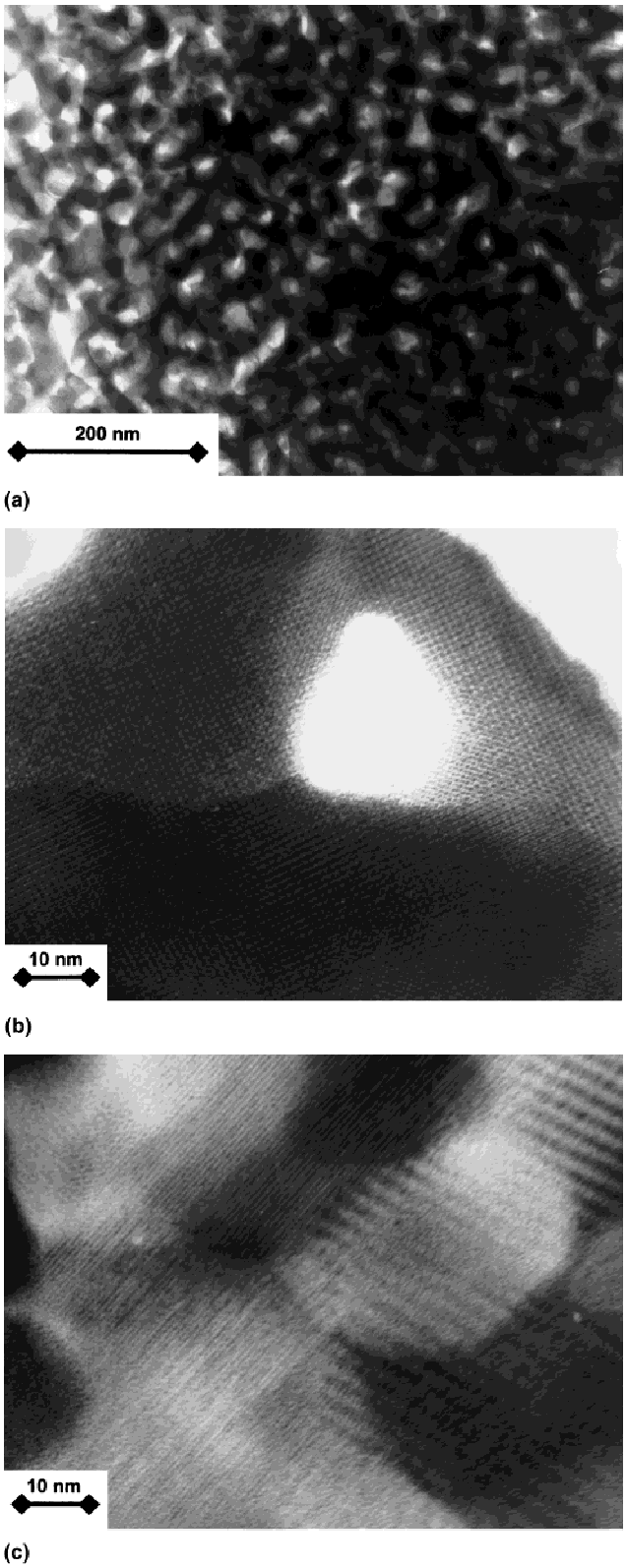

FIG. 10. (a) Nanoscale porosity in sol-gel-derived SBN50 powders [similar to the nanoscale porosity found for thin films in Fig. 7(b)]. (b) TEM HREM image of SBN50 powders in a region with the tetragonal tungsten bronze phase. (100), (010) *d* spacings of 1.24 nm can be observed. (c) TEM HREM image of SBN50 powders with the orthorhombic phase. Large fringes are moiré fringes from overlapping grains. A *d* spacing of 0.8 nm can be observed.

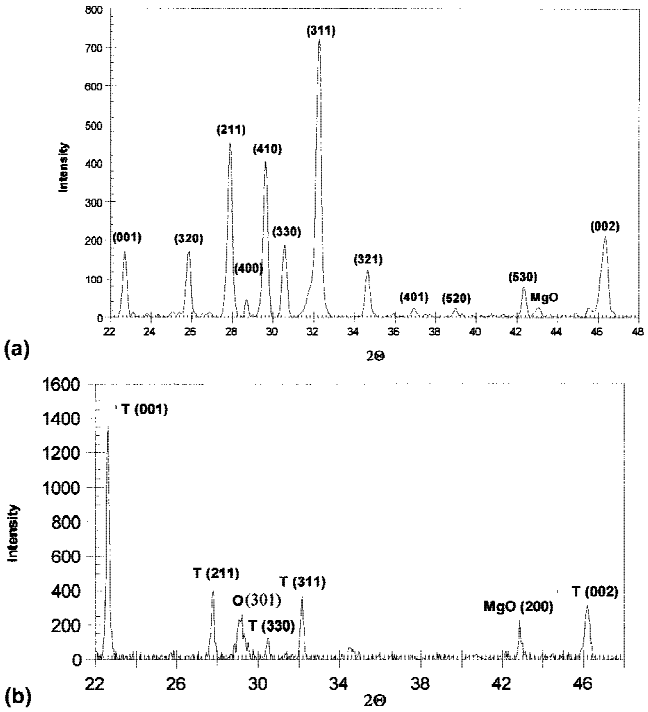

FIG. 11. XRD plots: (a) SBN73 thin films on (100) MgO substrate after controlled furnace annealing, (b) (001)-oriented SBN73 thin films on (100) MgO with some orthorhombic (O) $SrNb_2O_6$ phase present in addition to the tetragonal tungsten bronze (T) phase after fast thermal annealing.

out the solid solution for both powders and thin films on (111) Si substrates. The Ba/Sr ratio was the main factor determining crystal structure whereas choice of substrate has a less-pronounced effect.

(4) Increased (001) orientation of SBN was observed for films deposited on (100) MgO when fast thermally processed.

REFERENCES

1. M.P. Trubelja and D.K. Smith, J. Mater. Sci. **31,** 1435 (1996).
2. S.C. Abrahams and E.T. Keve, Ferroelectrics **2,** 129 (1971).
3. I.G. Ismailzade, Kristallografiya **5,** 268 (1960).
4. C.H. Luk, C.L. Mak, and K.H. Wong, Thin Solid Films **298,** 57 (1997).
5. P.B. Jamieson and J.L. Bernstein, J. Chem. Phys. **48,** 5048 (1969).
6. D. Viehleand, Z. Xu, and W. Huang, Philos. Mag. A **71,** 205 (1995).
7. G. Smolenskii, Y. Kzendzov, A. Agranovaskaya, and S. Popov, Solid State Phys. **2,** 244 (1959).
8. Y. Xu and J.D. Mackenzie, Integrated Ferroelectrics **1,** 17 (1992).
9. W. Sakamoto, T. Yogo, K. Ogiso, and S. Hirano, J. Am. Ceram. Soc. **79,** 2283 (1996).
10. O. Yamaguchi, K. Matsui, and K. Shimizu, J. Am. Ceram. Soc. **68,** C-173 (1985).
11. M.H. Francombe, Acta Crystallogr. **13,** 131 (1960).
12. J.R. Carruthers and M. Grasso, J. Electrochem. Soc. **117,** 1426 (1970).
13. L.A. Bursill and P.L. Lin, Acta Crystallogr., Sect. B. **43,** 49 (1987).
14. L.A. Bursill and P.J. Lin, Philos. Mag. B **54,** 157 (1986).